https://doi.org/10.36296/1819-8058.2026.1(84).145-154

NUMERICAL ESTIMATION OF THE SOLAR COPS PERFORMANCE OF A SINGLE-STAGE ABSORPTION REFRIGERATION MACHINE FOR AIR-CONDITIONING A BUILDING

Received Jan. 21, 2026; accepted Mar. 23, 2026
Available online Mar. 31, 2026

Mokhtari Fatima Z.[1], **Mokhtari Abderahman M.**[2], **Mekroussi Saïd**[3]

Author for correspondence: Mokhtari Fatima
e-mail: mokhtari_f19@yahoo.fr

[1] Student (Faculty of Mechanical Engineering)
https://orcid.org/0009-0002-4388-9957

[2] Professor (Laboratory of Soil and Thermal Materials, Faculty of Architecture and Civil Engineering)
https://orcid.org/0000-0002-9725-5995

[3] Professor (Laboratory of Industrial Technologies)
https://orcid.org/0000-0001-8824-3960

[1, 2] University of Science and Technology Mohamed Boudiaf (USTO), Oran, Algeria

[3] Ibn Khaldoun University, Tiaret, Algeria

Abstract. *This study numerically investigates a solar absorption chiller coupled with a cylindro-parabolic (parabolic-trough) collector to air-condition an amphitheater at Ibn Khaldoun University in Algeria's High Plateaus, specifically the city of Tiaret, whose astronomical coordinates recorded by the Ain Bouchakif meteorological station are: 35.21° N latitude, 1.28° E longitude, and 1000 m altitude, for a summer day in July. The hourly evaluation of the chiller's solar coefficient of performance (SCOP) over the summer day considered the region's solar irradiance and the thermal characteristics of the solar collector, whose geometric and physical properties were selected for this purpose. The solar COP obtained for our system reached approximately 0.4736, a considerable and acceptable value.*

Key words: *concentrator; thermal efficiency; absorption; solar radiation; cooling; cylindro-parabolic; COP; absorber; Capderou; heat transfer fluid.*

ЧИСЕЛЬНА ОЦІНКА СОНЯЧНОГО КОЕФІЦІЄНТА ПРОДУКТИВНОСТІ (COPS) ОДНОСТУПЕНЕВОЇ АБСОРБЦІЙНОЇ ХОЛОДИЛЬНІЙ МАШИНИ ДЛЯ КОНДИЦІЮВАННЯ БУДІВЛІ

Отримано 21 січ. 2026 р.; рекомендовано до публікації 23 бер. 2026 р.
Доступно онлайн 31 бер. 2026 р.

Мохтарі Фатіма З.[1], **Мохтарі Абдерахман М.**[2], **Мекруссі Саїд**[3]

Автор для кореспонденції: Балу Пандіан,
e-mail: balumitauto@gmail.com

[1] студент ф-ту машинобудування
https://orcid.org/0009-0002-4388-9957

[2] професор лабораторії матеріалів, ґрунтів і теплотехніки, ф-т архітектури та цивільної інженерії
https://orcid.org/0000-0002-9725-5995

[3] Професор лабораторії промислових технологій
https://orcid.org/0000-0001-8824-3960

[1, 2] Університет науки і технологій імені Мохамеда Будіафа (USTO), Оран, Алжир

[3] Університет Ібн Хальдуна, Тіарет, Алжир

Анотація. *У цьому дослідженні здійснено чисельний аналіз продуктивності сонячної абсорбційної холодильної машини, поєднаної з циліндропараболічним (параболоциліндричним) колектором, для кондиціювання амфітеатру Університету Ібн Хальдуна у регіоні Високих плато Алжиру, а саме в місті Тіарет, астрономічні координати якого, зафіксовані метеорологічною станцією Айн-Бушакіф, становлять: 35,21° пн. ш., 1,28° сх. д., висота – 1000 м над рівнем моря, для літнього дня в липні. Погодинне оцінювання сонячної продуктивності холодильної машини (COP) протягом літнього дня здійснювали з урахуванням показників сонячного опромінення в регіоні та теплових характеристик сонячного колектора, геометричні й фізичні параметри якого були обрані для цієї мети. Отримане для системи значення сонячного коефіцієнта продуктивності (COP) становило приблизно 0,4736, що є досить значним і прийнятним показником.*

Ключові слова: *концентратор; теплова ефективність; абсорбція; сонячне опромінення; охолодження; циліндропараболічний; COP; абсорбер; модель Капдеру; теплоносій.*

Abbreviations

I_b – Direct solar irradiation $[\mathrm{W\,m^{-2}}]$
T_L – Linke turbidity factor
q_u – Useful energy transferred to the heat-transfer fluid
F_R – Heat-removal factor
F' – Collector efficiency factor
η_{opt} – Optical efficiency of the concentrator
η_{th} – Thermal efficiency of the concentrator
A_0 – Collector aperture area $(\mathrm{m^2})$
A_r – Outer surface area of the absorber tube $(\mathrm{m^2})$
A_v – Glass envelope surface area $(\mathrm{m^2})$
D_i – Inner diameter of the absorber (m)
D_o – Outer diameter of the absorber (m)
σ – Stefan–Boltzmann constant $5.66897 \times 10^{-8}\,\mathrm{W\,m^{-2}\,K^{-4}}$
ε_r – Absorber emissivity
ε_v – Glass emissivity
T_{amb} – Ambient temperature (K)
T_{ab} – Absorber temperature (K)
T_i – Inlet temperature of the heat-transfer fluid (oil) (K)
T_v – Glass temperature (K)
P – Pressure $[\mathrm{bar}]$
U_L – Overall heat-loss coefficient $[\mathrm{W\,m^{-2}\,K^{-1}}]$
h_c – Convective heat-transfer coefficient $[\mathrm{W\,m^{-2}\,K^{-1}}]$
h_r – Radiative heat-transfer coefficient $[\mathrm{W\,m^{-2}\,K^{-1}}]$
Q – Heat transfer rate $[\mathrm{W}]$
h – Enthalpy $[\mathrm{J\,kg^{-1}}]$
K_F – Thermal conductivity of the heat-transfer fluid $[\mathrm{W\,m^{-1}\,K^{-1}}]$
V – Wind speed $(\mathrm{m\,s^{-1}})$
C_p – Specific heat at constant pressure $[\mathrm{J\,Kg^{-1}\,K^{-1}}]$
X – Solution concentration

Introduction

Using solar energy for air-conditioning is a promising approach because peaks in cooling demand generally coincide with maximum solar irradiance. Moreover, solar-thermal air-conditioning systems reduce electricity consumption, allow the use of environmentally friendly refrigerants, minimize noise, and simplify electrical infrastructure, particularly in rural areas.

In December 2009, more than thirty 50 MW plants based on cylindro-parabolic mirror technology and a 17 MW tower plant (with 15 h of storage) were under construction in Spain [1]. By 2017, Spain accounted for nearly half of global capacity, at 2300 MW, making it the world leader in deploying concentrating solar-thermal power plants. The United States followed with 1740 MW [2]. The largest concentrating solar-thermal projects worldwide include the "IVANPAH" solar facility (392 MW) in the United States, which uses solar-tower technology, and the "MOJAVE SOLAR" project (354 MW) in the United States, which uses parabolic-trough concentrators [2].

Numerical studies and numerous experimental works have addressed the coefficient of performance of refrigeration equipment, particularly solar refrigeration. For example, Cascales et al. [3] developed several models of $LiBr/H_2O$ solar absorption refrigeration equipment. O. Kizilkan et al. [4] improved the cost-effectiveness of such equipment by establishing optimal standards. Romero et al. [5] conducted a comparative performance study of a reversible absorption heat-pump system using the mixtures ($LiBr/H_2O$) and (KOH + NaOH + CsOH). The results showed similar performance for both mixtures and noted that the (KOH + NaOH + CsOH) mixture operates over extended temperature ranges for the condenser and absorber.

In this context, our work estimates the solar performance of a single-stage absorption refrigeration machine driven by thermal energy transferred from a cylindro-parabolic collector with carefully selected geometric and optical characteristics, under the climatic conditions of the Tiaret region, Algeria, for a summer day in July.

Solar Modelling

In the literature, several authors have proposed empirical relations linking meteorological variables to radiometric parameters (global, diffuse, and direct illuminance). For the present work, we adopt the Capderou model **[6]**, which relies on attenuation coefficients of solar radiation by atmospheric constituents to compute the direct component of solar irradiation received on an inclined plane under clear-sky conditions.

$$I_b = I_C \exp\left[-T_L\left(0.9 + \frac{9.4}{0.89^Z}\sin(h)\right)^{-1}\right]\cos(\theta)$$

with I_C the Earth–Sun distance factor:

$$I_C = I_0\left[1 + 0.0033\cos\left(\frac{360}{365}n\right)\right]$$

I_0 is the solar constant $= 1367$.
$\cos(\theta)$, the cosine of the incidence angle, varies with the solar tracking mode. In our case, full solar tracking is used; hence $\cos(\theta) = 1 \Rightarrow \theta = 0$.
T_L is the Linke turbidity factor.

Thermal Modelling of a Parabolic-Trough Concentrator (PTC)

The solar irradiance estimated in the previous section is captured by an inclined cylindro-parabolic concentrator equipped with a tracking system so that the incident rays remain perpendicular to the concentrator's aperture plane.

We modelled this collector using heat-transfer equations among the absorber's components (Fig. 1). To simplify the model, we adopt the following assumptions:

- The PTC has a tracking system that perfectly follows the sun throughout the day.
- Transverse conduction within the absorber and within the glass envelope is negligible.
- A vacuum is maintained between the absorber tube and the glass envelope.
- Solar radiation is uniformly distributed within the absorber.
- Conduction heat exchange within the absorber and within the glass envelope is negligible.
- The heat-transfer fluid is incompressible.
- The parabolic geometry is symmetric.

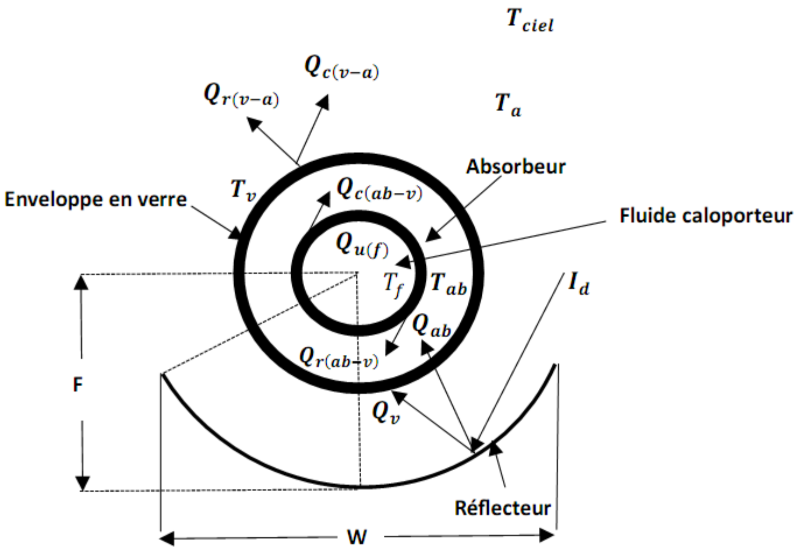

Fig. 1. Heat fluxes exchanged in the parabolic-trough collector (PTC) [7]

Thermal efficiency (η_{th}) [7,13] is the ratio between the useful heat transferred to the heat-transfer fluid and the direct solar power incident on the collector surface (PTC):

$$\eta_{\text{th}} = \frac{q_u}{A_0\, I_b}$$

The useful power gained by the fluid in the concentrator is given by [8]:

$$q_u = F_R[\eta_{\text{opt}}\, A_0\, I_b \; - \; U_L\, A_r\, (T_i - T_{amb})]$$

The heat removal factor $F_R$can be computed from [10,11]:

$$F_R = \frac{\dot{m}C_P}{A_0\;U_L}\left(1 - e^{\left(\frac{A_0 U_L F'}{\dot{m}C_P}\right)}\right)$$

The optical efficiency $\eta_{\text{op}}$of the concentrator is [8,12]:

$$\eta_{\text{op}} = \rho_0\, \alpha_0\, \gamma\, K$$

With the incidence-angle modifier Kgiven by [7,9]:

$$K = 1 - 0.00384\,(\theta) - 0.000143\,(\theta)^2$$

The overall heat-loss coefficient $U_L$is calculated as [10, 11]:

$$U_L = [\;\frac{A_{ab}}{(h_w + h_{r,v-amb})\, A_v} \; + \; \frac{1}{h_{r,ab-v}}\;]^{-1}$$

Here, $h_w$is the external convection coefficient between the glass and ambient air, with wind speed V(m s^-1^), computed as [10]:

$$h_w = 5.7 + 3.8\, V$$

The radiative exchange coefficient between the glass and ambient air is [10, 11]:

$$h_{r,v-amb} = \varepsilon_{ab}\, \sigma\, (T_v + T_{amb})\, (T_v^2 + T_{amb}^2)$$

The radiative exchange coefficient between absorber and glass is [10,11]:

$$h_{r.ab-v} = \frac{\sigma(T_v + T_{ab})(T_v^2 + T_{ab}^2)}{\frac{1}{\varepsilon_{ab}} + \frac{A_{ab}}{A_v}\left(\frac{1}{\varepsilon_v} - 1\right)}$$

The mirror efficiency factor $F'$is determined as [10, 11]:

$$F' = \frac{\frac{1}{U_L}}{\frac{1}{U_L} + \frac{D_0}{h_{fi} D_i} + \left(\frac{D_0}{2K_F}\ln\frac{D_0}{D_i}\right)}$$

The internal convection coefficient of the absorber is [10]:

$$h_{fi} = \frac{Nu\, K_F}{D_i}$$

As shown schematically in Fig. 2(a), the parabolic-trough concentrator is coupled to a single-stage H_2O–LiBr absorption chiller. Thermal energy is delivered via a circulating heat-transfer fluid, driven by a pump, to ensure heat exchange in the generator between the H_2O–LiBr solution and the heating water. The refrigeration cycle operates through the chemical absorption of the H_2O/LiBr solution, governed by the operating temperatures and pressures of each subsystem component.

An absorption system, Fig. 2(b), comprises first the set (condenser, expansion valve, evaporator) through which only the pure refrigerant circulates. This set is connected to the chemical section of the process, which alters the state of the evaporated refrigerant so that it becomes condensable at the temperature of the environment.

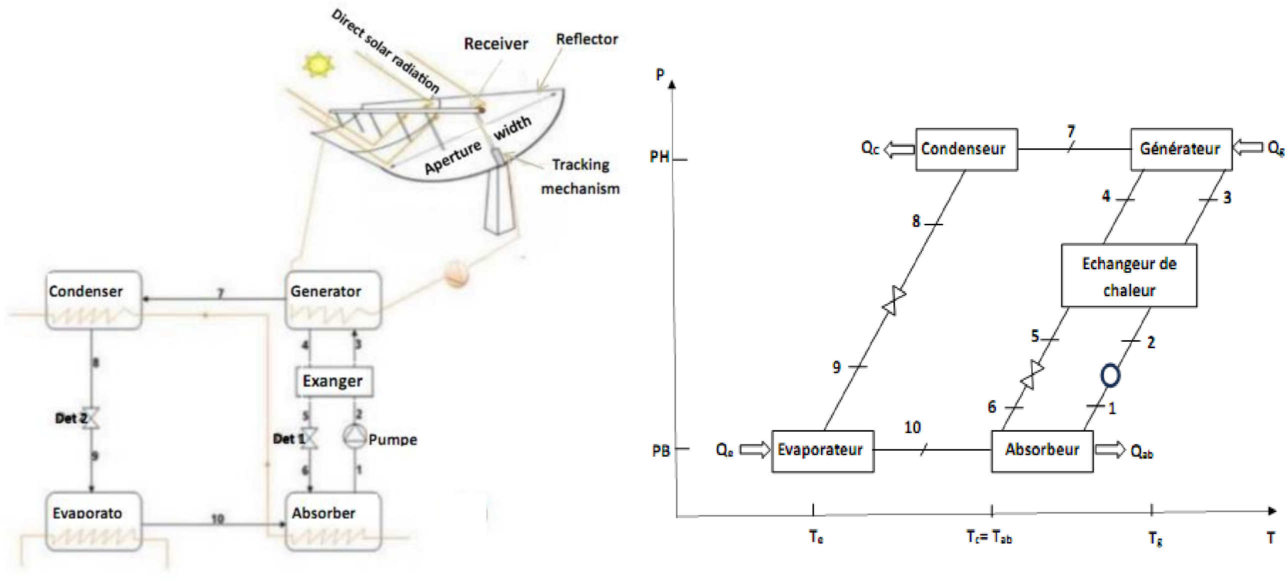

a) *b)*

Fig. 2. (a) Schematic of a solar absorption refrigeration system coupled with a solar collector. (b) Pressure–temperature diagram for the refrigeration cycle

Two balances – mass and solute concentration – can be written at the absorber (Fig. 3):

$m_f + m_g - m_a = 0$ (overall H_2O-LiBr–solution balance),
$m_g\, X_c - m_a\, X_d = 0$ (LiBr balance),
where X_c is the mass fraction (title) of the concentrated solution leaving the generator and entering the absorber, and X_d is the mass fraction of the binary mixture, rich in refrigerant, leaving the absorber and entering the generator.

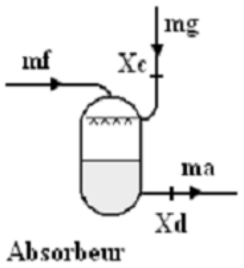

Fig. 3. Absorber balances

Enthalpy balances for each component

- Condenser: $Q_c = m_f\,(h_8 - h_7)$
- Evaporator: $Q_e = m_f\,(h_{10} - h_9)$
- Generator: $Q_g = m_f\, h_7 + m_g\, h_4 - m_a\, h_3$
- Absorber: $Q_a = m_g\, h_6 + m_f\, h_{10} - m_a\, h_1$
- Pump: $W = m_a\,(h_2 - h_1)$

Flow ratio

The Flow ratio FR (specific flow rate of the H_2O-LiBr solution) is defined as

$$FR = \frac{X_c}{X_c - X_d} = \frac{X_6}{X_6 - X_1}$$

Coefficient of performance (COP)

The COP of the absorption machine is then

$$COP = \frac{Q_e}{Q_g + W_P} = \frac{(h_{10} - h_9)}{h_7 + (FR - 1)h_4 - FR(h_3 + h_1 - h_2)}$$

Thermophysical property calculations (H_2O–LiBr)

To evaluate performance, the thermodynamic properties (pressure, enthalpy, concentration) of the H_2O-LiBr pair at each cycle state point were computed from the thermodynamic relations derived from the analytical Gibbs-energy formulation, as follows.

1. Saturation pressure of water (high and low), Dupré formula [14]

$$P_{eq} = P_c exp(\frac{T_c}{T_k}\sum\alpha)$$

With

- $\alpha = \frac{T_c}{T_k}(-7.85823\, T_0 + 1.83991\, T_0^{1.5} - 11.7811\, T_0^{3} - 22.6705\, T_0^{3.5} - 15.9393\, T_0^{4} + 1.77516\, T_0^{7.5})$
  $T_0 = 1 - \frac{\mathrm{T_k}}{\mathrm{T_c}}$
- $\mathrm{T_c} = 647.14C°$
- $\mathrm{T_k} = T + 273.15$
- $\mathrm{P_c} = 22064Kpa$
- **Enthalpy of water (refrigerant) as a fun**

- **ction of temperature, $\boldsymbol{h(T)}$**
- **Liquid enthalpy** h_{liq}[15]

$\mathrm{h_{liq}(T) = C_P . T}$

Where Cp = 4.185 2 (Kj/Kg °C)

- **Saturated-vapor enthalpy** $h_{\text{vap}}(T)$[16]

$$h_{\text{vap}}(T) = -125397 \times 10^{-8}\, T^2 + 1.88060937\, T + 2500.55$$

- **Superheated-vapor enthalpy** $h_{\text{surch}}(T,P)$[17]

$$h_{\text{surch}}(T) = \frac{(h_{sh2} - h_{sh1})\, T}{100} + h_{sh1}$$

Equilibrium pressure of the H_2O/LiBr **mixture $\boldsymbol{P(T,X)}$**[17]

$$\log P = C + \frac{D}{T_r + 273.15} + \frac{E}{(T_r + 273.15)^2}$$

with, $C = 7.05$, $D = -1596.49$, $E = -104095.5$, and

- $\mathrm{T_r} = \frac{-2\mathrm{E}}{(\mathrm{D}+[\mathrm{D}^2-4\mathrm{E}(\mathrm{C}\log\mathrm{P})]^{0.5})-273.15}$
- $T_{\text{sol}} = \sum B + T_r \sum A$

Mixture enthalpy $\boldsymbol{h(T,X)}$for H_2O/LiBr [17]

- For $0\% < X < 40\%$:

$$h = [A_0X^0 + A_1X^1 + A_2X^2 + CT\,(B_0X^0 + B_1X^1 + B_2X^2)] \times 3.326$$

where , $CT = (\frac{9}{5}T) + 32$

- For $40\% < X < 70\%$:

$$h = \sum A + T\sum B + T^2 \sum C$$

Mixture density $\boldsymbol{d_{\text{LiBr}}(T,X)}$[18]

$$d_{\text{LiBr}} = \frac{1145.36 + 470.84X + 1374.79\, X^2}{1000} - (33.3393 + 0.51749\, X)\,\frac{T + 273.15}{100000}$$

Results and Discussion

The thermal and dynamic calculations for our system were performed using a computational code implemented in MATLAB. The geometric and optical characteristics of the collector were carefully selected from the parabolic-trough (CCP/PTC) data provided by Sandia National Laboratories (SNL) and are reported in Table [7].

Table. Optical and geometric characteristics of the studied solar concentrator

Characteristic	Value
Mirror length L(mm)	7800
Mirror width l(mm)	5000
Absorber outer diameter D_o(mm)	70
Absorber inner diameter D_i(mm)	66
Glass envelope outer diameter DV_o(mm)	115
Glass envelope inner diameter DV_i(mm)	109
Absorber-tube emissivity	0.14
Glass-envelope emissivity	0.89
Intercept factor γ	0.92
Mirror reflectance ρ_m	0.92
Glass transmittance ε_v	0.95
Absorber absorptance α_{ab}	0.904

Fig. 4 shows the evolution of solar irradiance from sunrise to sunset on 3 July 2025. Solar irradiance was computed using the Capderou model [6], which is the reference model most commonly used in the Algerian atlas. As indicated in the figure, at noon the global solar irradiance reaches 1100 W·m^{-2}, while the direct component attains 975 W·m^{-2}; by 19:00, irradiance drops to 2 W·m^{-2}. Overall, the calculations yield satisfactory radiative results, supporting the design and deployment of a solar-collector field sized as needed for the study area.

The optical efficiency of the solar collector is directly determined by the concentrator's geometric and optical properties. As shown by the thermal-efficiency formulation, several terms act directly on the parabolic-trough's optical efficiency. Some are intrinsic to design and manufacture—most notably the intercept factor $\boldsymbol{\gamma}$, which sets the fraction of direct solar radiation captured by the absorber tube and is on the order of 95%. Mirror reflectance $\boldsymbol{\rho_m}$is likewise high (≈ 95%) and depends on mirror cleanliness. The glass-envelope transmittance $\boldsymbol{\tau}$ for solar radiation is also around 95%, while the absorber absorptance $\boldsymbol{\alpha_{ab}}$ governs the portion of direct solar input actually absorbed. These values do not account for additional influences with immediate impact, including environmental soiling (dust), alignment or assembly errors, and related factors.

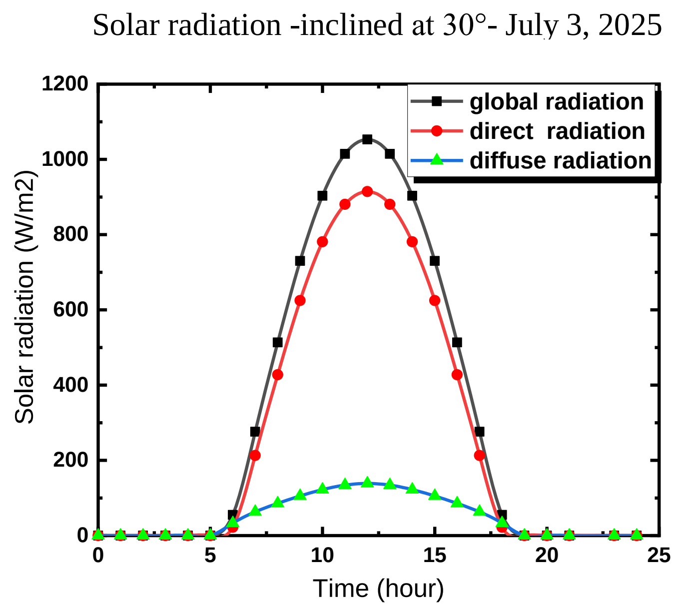

Fig. 4. Solar irradiance profile for 3 July 2025

From Fig. 5, the optical efficiency η_{opt}reaches 77.52%, the highest value obtained by the collector, and remains essentially stable over the day owing to continuous solar tracking. The maximum thermal efficiency η_{th}attains 65.27% at 12:30, corresponding to the peak of useful energy delivered by the concentrator.

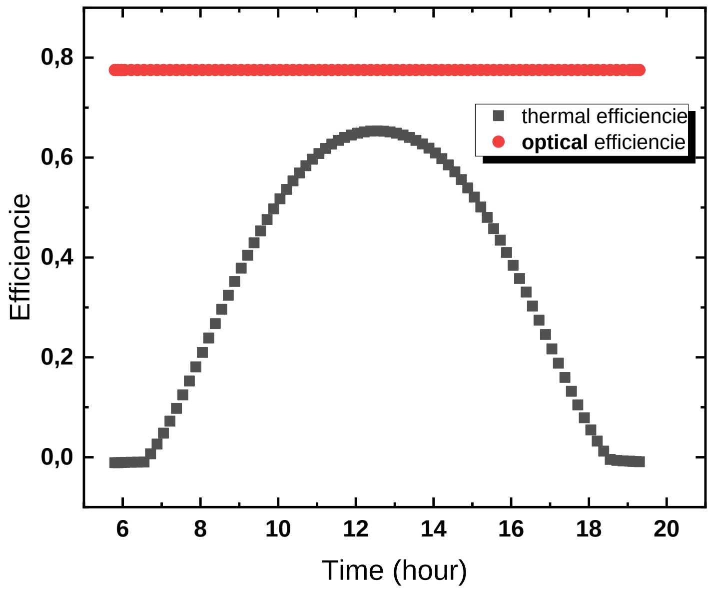

Fig. 5. Diurnal evolution of the parabolic-trough collector's (PTC) optical and thermal efficiencies on 3 July 2025

Fig. 6 shows the time evolution of the heat-removal factor $F_R$and the collector efficiency factor F'over the study day, from sunrise to sunset. The coefficient $F'$is defined as the thermal resistance between the absorber and the ambient relative to the resistance between the fluid and the ambient. In this study, $F'$was 0.6471 at sunrise, 0.5399 at midday, and 0.6506 at sunset.

Regarding F_R, it is presented here as the mirror efficiency factor, expressing the ratio of the actual energy transfer to the maximum possible transfer. It is known that $F_R$varies with two parameters—F' and the overall loss coefficient U_L. According to Figure 6, F_R and F'evolve in parallel, although F'shows the larger relative variation. We observe $F_R = 0.6421$at sunrise, a minimum of 0.5287 at mid-day, and 0.6450 at sunset.

Coating the absorber tube with a transparent surface reduces heat loss between the absorber and the glass envelope. It retains more of the incident solar radiation and limits its dissipation to ambient air by radiation and thermal convection, since the glass is opaque to the long-wave emission from the absorber. To further limit these losses, one may use a selective surface on the absorber tube or create an evacuated annulus between the absorber and the glass envelope to suppress convection and conduction.

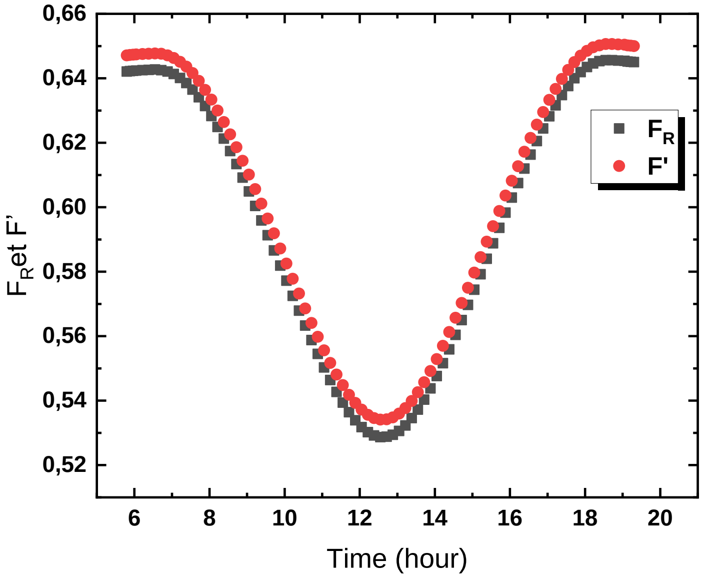

Fig. 6. Evaluation of the heat-removal factor (F_R) and the mirror efficiency factor (F’)

As shown in Fig. 7, the overall thermal loss coefficient U_L peaks at 7.513 W/m²·K at 12:30, and decreases to 4.352 W/m²·K at the beginning and end of the day. This is significant; mitigation requires assessing direct solar irradiance, outdoor air temperature, and wind speed. These drivers are necessary to improve collector performance and efficiency.

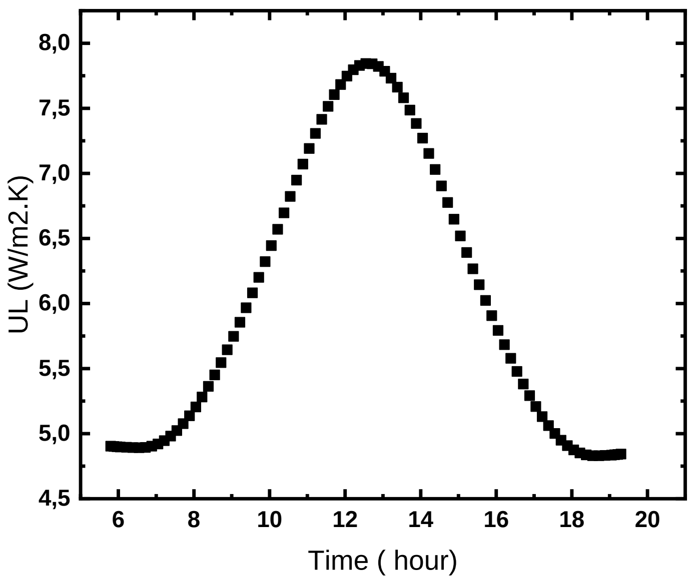

Fig. 7. Evaluation of the overall heat-loss coefficient (U_L) as a function of time

To validate our single-stage H_2O–LiBr absorption chiller model, we compared our computed COP (Fig. 8) with the results reported by Romero et al. [5]. The selected operating temperatures are:

- Generator temperature T_g: 65–90 °C
- Condenser temperature T_c: 43 °C
- Absorber temperature T_a: 40 °C
- Evaporator temperature T_e: 7–10 °C
- Heat-exchanger effectiveness: $\eta = 0.70$

The agreement between our calculations and the literature values is good, supporting the fidelity of the implemented model.

Fig. 9 shows how the coefficient of performance (COP) varies with generator temperature T_g, for $T_a = 40°\text{C}$, $T_c = 43°\text{C}$, $T_e = 7°\text{C}$, and heat-exchanger effectiveness $= 0.70$. The COP increases roughly linearly between 80 and 90 °C. From about 95 °C, it tends to level off and reaches a stable value of 0.71 once $T_g > 105°\text{C}$. Near 110 °C, crystallization (“gelling”) begins as solids form and block fluid circulation. To prevent this, control the salt concentration, use efficient pumps and heat exchangers, and keep both temperature and flow rate within their safe operating ranges.

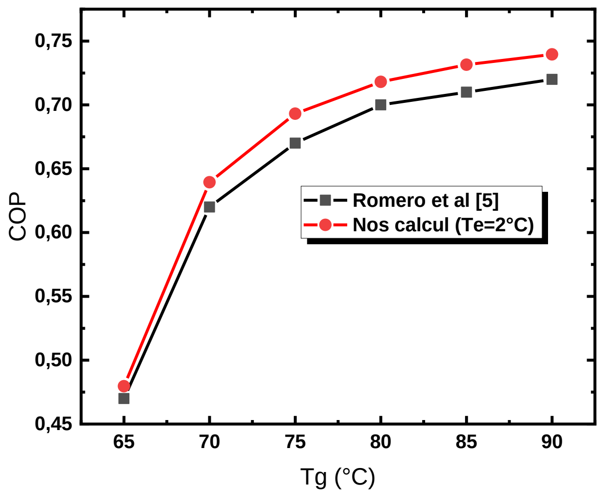

Fig. 8. Comparison of our results with those of Romero and al. [5]. Conditions: $T_a = 30°C$, $T_c = 30°C$, $T_e = 2°C$, heat-exchanger effectiveness $(EFF) = 0\%$

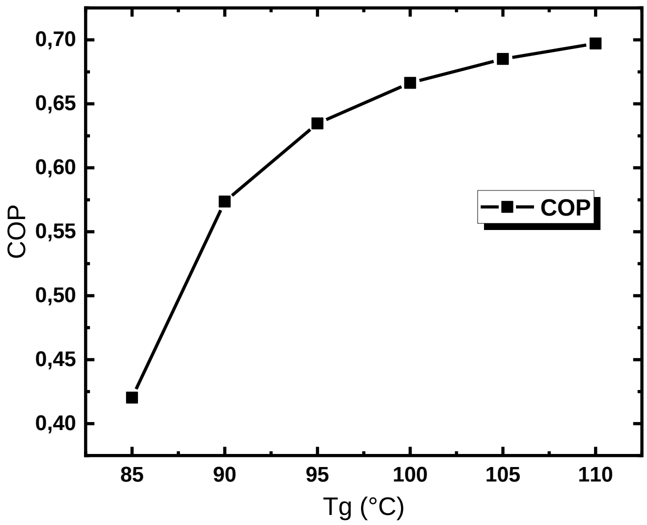

Fig. 9. COP versus generator temperature

Fig. 10 shows the variation of the coefficient of performance (COP) with evaporator temperature T_e for different generator temperatures T_g. COP increases as the evaporation temperature rises. In addition, higher generator temperatures yield a higher COP for the machine.

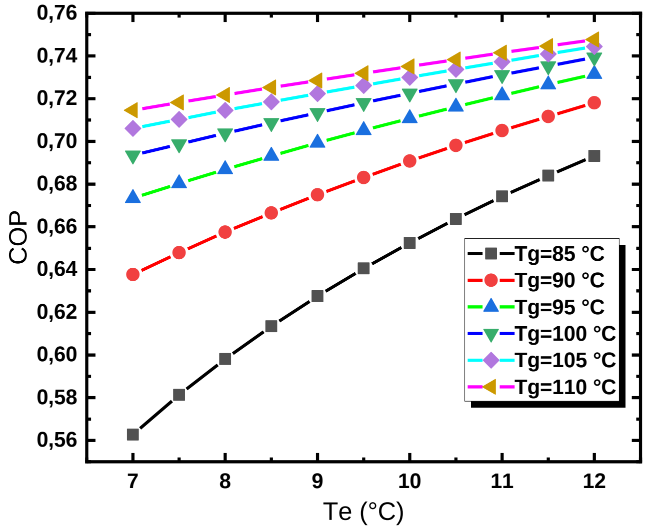

Fig. 10. COP versus T_e for different T_g values. Conditions: $T_a = 40°C$, $T_c = 42°C$, heat-exchanger effectiveness $= 0.70$

Fig. 11 illustrates the performance of the solar absorption refrigerator over a July summer day. The solar coefficient of performance (SCOP) peaks at 0.4736 at noon, when irradiance is highest, and falls to zero at sunrise and sunset. This pattern underscores the system's dependence on the intensity of solar radiation intercepted by the concentrator throughout the day.

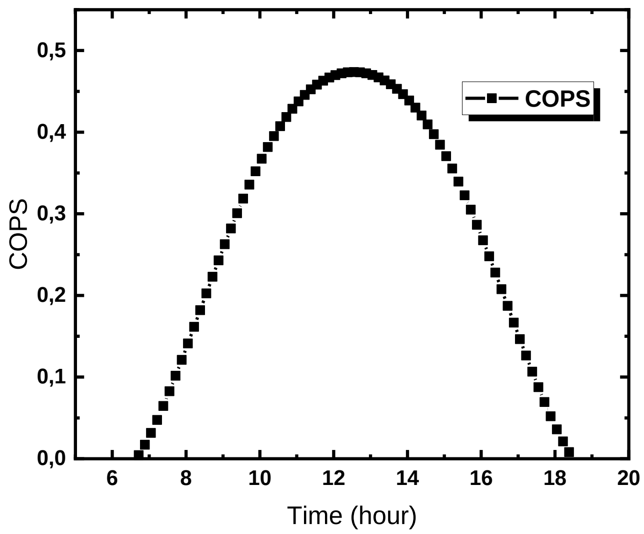

Fig. 11. Time profile of SCOP on 3 July 2025

Conclusion

This study develops a dynamic simulation of a single-stage solar absorption cooling system using the water–lithium bromide (H_2O–LiBr) pair to cool a conference room scheduled for the summer day 03/07/2025. We first formulated a mathematical model for the cylindro-parabolic collector and another for the cooling subsystem. Balance equations were written for every component in both units, and a MATLAB program was implemented to simulate system behaviour under the site's specific climatic conditions. We then examined diurnal variations in solar irradiance, the collector's thermal efficiency η_{th}, the heat-removal factor F_R, the collector efficiency factor F', and the overall heat-loss coefficient U_L. Finally, we validated the computed coefficient of performance (COP) by analysing its sensitivity to generator and evaporator temperatures, with the aim of characterising the time evolution of the solar coefficient of performance over the study day.

Findings:

- The global solar irradiance I_G reached a daytime maximum of ≈ 1100 $W{\cdot}m^{-2}$.
- The collector's maximum thermal efficiency $\eta_{th}$was 65.27%, and the optical efficiency $\eta_{op}$was 77.52%.
- The heat-removal factor $F_r$and the collector efficiency factor F'evolved in parallel; the maximum $F'$was 0.6506 early in the day, while at noon it was 0.5399.
- The overall heat-loss coefficient $U_L$peaked at ≈ 7.513 $W{\cdot}m^{-2}{\cdot}K^{-1}$.
- The calculated COP values agree with Romero et al.; the maximum COP was 0.71.
- As evaporator temperature increases, COP increases; higher generator temperatures further enhance performance.
- The highest solar performance (SCOP) at noon was 0.4736.
- The maximum solar performance (SCOP) attained by the system was 0.4736.

REFERENCES

1. Sofiane Bouaichaoui , L'électricité d'origine solaire :Les centrales solaires thermodynamiques ; , bulletin_018_06, Centre de Développement des Energies Renouvelables (CDER)
2. Mokhtar GHODBANE,' Thermal Numerical Examination of a Linear Solar Collector: the Parabolic Trough Concentrator (PTC) , as a Case Study', Unité de Recherche Appliquée en Energies Renouvelables, Ghardaïa – Algeria 24 - 25 Octobre 2018
3. J.R.G Cascales, F.V García, J.M.C Izquierdo, J.P.D Marín and R. Martínez Sánchez, "Modelling an absorption system assisted by solar energy", Applied Thermal Engineering, vol. 31, pp. 112D118, 2011
4. O. Kizilkan, A. Sencan and S.A. Kalogirou, "Thermoeconomic optimization of a LiBr absorption refrigeration system", Chemical Engineering and Processing, vol. 46, pp. 1376D1384, 2007
5. R.J. Romero, W. Rivera, J. Garacia and R. Best, "Theoretical comparison of performance of an absorption heat pump system for cooling and heating operating with an aqueous ternary hydroxide and

water/lithium bromide”, Applied Thermal Engineering, Vol. 21, pp. 1137D1147, 2001.

6. Capderou. M, 1987. Atlas Solaire de l’Algérie, Modèles Théoriques et Expérimentaux.Volume1, Tome 2; Office des Publications Universitaires, Algérie
7. Garcia-Valladares, O, Velazquez. N, 2009. Numerical simulation of parabolic trough collector: improvement using counter flow concentric circular heat exchangers
8. S. A. Kalogirou, Solar Energy Engineering: Processes and Systems, 1st ed. Academic Press, 2009
9. Soteris A. Kalogirou* ‘Solar thermal collectors and applications’, Progress in Energy and Combustion Science 30 (2004) 231–295
10. J. A. Duffie and W. A. Beckman, Solar Engineering of Thermal Processes, 4th ed. Wiley, 2013
11. M. Ghodbane, B. Boumeddane, and N. Said, "A linear Fresnel reflector as a solar system for heating water: theoretical and experimental study," Case Studies in Thermal Engineering, vol. 8, no. C, pp. 176-186,
12. M. Ghodbane, B. Boumeddane, S. Largot, and H. Berkane, "Modélisation d'un cycle de réfrigération solaire à éjecteur couplée à un concentrateur cylindro-parabolique," in International Conférence en Clean Cooling Technologies in the ME NA Regions (ICT3_MENA'2015) Bou Smail, W. Tipaza, 5-6 October 2015
13. M. Ghodbane, B. Boumeddane, N. Moummi, S. Largot, and H. Berkane, "Study and numerical simulation of solar system for air heating," Journal of Fundamental and Applied Sciences, vol. 8, no. 1, pp. 41- 60, http://dx.doi.org/10.4314/jfas.v8i1.3, 2016
14. J. Patek, J. Klomfar. A computationally effective formulation of the thermodynamic properties of LiBr–H2O solutions from 273 to 500 K over full composition range. International Journal of Refrigeration 29 (2006) 566–578
15. Da-Wen Sun. thermodynamic design data and optimu design maps for absorption refrigeration systems. National University of Ireland. August 1996
16. Rogers GFC, Mayhew YR. Thermodynamic and transport properties of fluids: SI units. 4th ed. UK: Blackwell Publishers; 1992
17. ASHRAE, Handbook of Fundamentals.Atlanta, 1997
18. Lee RJ, DiGuilio RM, Jeter SM, Teja AS. Properties of lithium bromide–water solutions at high temperatures and concentration. II. Density and viscocity. ASHRAE Trans 1990;96(Pt. 1):709–28